15ÈMES JOURNÉES DE L'HYDRODYNAMIQUE
22 - 24 novembre 2016 - Brest

STABILITE DE ROUTE DES NAVIRES TRACTES PAR CERF-VOLANT

COURSE KEEPING OF SHIP TOWED BY KITE

N. Bigi[1,2], M. Behrel[1], K. Roncin[1], J. B. Leroux[1], A. Nême[1], C. Jochum[1], and Y. Parlier[3]

[1]ENSTA Bretagne, FRE CNRS 3744, IRDL, F-29200 Brest, France
[2]Contact: nedeleg.bigi@ensta-bretagne.org
[3]Beyond the sea, 1010 avenue de l'Europe, 33260 La Teste de Buch, France

Abstract

Towing a ship with a kite enables fuel saving. However, a dynamic kite flight can alter the ship equilibrium. The course-keeping relative to a true wind angle may be an issue. Consequently, a dynamic model of ship with kinematic kite model is developed. The ship dynamic model is based on a parametric maneuvering model. This model is validated through full scale trials of 13 m long fishing vessel. The comparison between the experiments and the model are satisfactory. Subsequently, a study on the influence of the longitudinal position of the tether attachment point is proposed. From a simplified method based on the ship maneuvering model, the drift angle is evaluated and an objective function to optimize the kite flight trajectory is determined. This function takes into account the ship resistance induced by the drift. For the case of study, the kite trajectory is optimized for a sailing at 135° of true wind angle and at the ship cruising speed. The computation of the motions shows that the more the tether attachment is backward, the more the propeller power required is low. Indeed, with a tether attachment point backward, the yaw balance requires that the rudder apply a transverse force opposed to the kite transverse force. Therefore, the drift angle is lower. Between two tether attachment points spaced of 3.2 m, the power saving is 8.85 % for the forward position and is 84.71 % for the backward position. This paper shows the high sensibility of the tether attachment position on the course-keeping and the performance. Due to the dynamic perturbations induced by the kite, an alternative rudder angle is required to follow an heading. For a given autopilot, the results shows that it exists an optimal tether attachment point to limit the rudder angle amplitude required for course keeping.

Résumé

La traction des navires par cerf-volant permet d'économiser du carburant. Cependant, le vol dynamique de cerf-volant peut modifier sensiblement l'équilibre d'un navire, et le suivi d'un cap par rapport au vent peut être problématique. Ainsi un modèle dynamique de navire avec un modèle cinématique de cerf-volant est développé. Le modèle de dynamique du navire est basé sur un modèle paramétrique de manoeuvrabilité. Ce modèle est validé avec des essais de manoeuvrabilité effectué à l'échelle réel sur un navire de pêche canadien de 13 m de long. La comparaison entre le modèle et les résulats experimentaux sont satisfaisant. Par la suite, une étude de l'influence de la position longitudinale sur le navire du point d'attache des lignes du cerf-volant est proposée. A partir d'une méthode simplifiée basée sur le modèle dynamique du navire, l'angle de dérive est évalué et une fonction d'optimisation prenant en compte la résistance induite par la dérive est dévelopée. Pour le cas d'étude, la trajectoire du cerf-volant est optimisée pour une navigation à 135° du vent réel et à la vitesse de croisière du navire. Par la suite le calcul des mouvements du navire montre que plus le point d'attache est reculé, plus la puissance de l'hélice nécessaire à l'avancement est faible. En effet, quand le cerf-volant est attaché plus en arrière, l'équilibre en lacet impose que le safran exerce un effort transverse opposé à celui du cerf-volant ce qui permet de diminuer l'angle de dérive. Entre deux positions espacées de 3.2 m l'économie de puissance nécessaire à l'avancement est de 8.85% pour la position d'attache de cerf-volant la plus avancée et de 84.71% pour la position plus réculée. A cause des perturbations induites par le cerf-volant sur le navire, une oscillation de l'angle de safran est nécessaire pour suivre un cap. Les résultats montrent qu'il existe une position d'attache optimale pour limiter l'amplitude d'angle barre nécessaire à la stabilité de route.

Nomenclature

$\mathcal{R}$ Coordinates system

$\underline{\underline{A}}$ Added mass matrix

$\underline{\underline{B}}$ Generalized mass matrix (6x6)

$\underline{\underline{C}}$ Centripetal matrix

$\underline{\underline{M}}$ Generalized mass matrix (6x6)

$\underline{F}$ Generalized force vector

$\underline{U}$ Velocity (3x1)

$\underline{V}$ Generalized velocity (6x1)

A Tether attachment point on the ship

A_K Kite area

C_B Hull block coefficient

C_{L_K} Kite lift coefficient

C_{WP} Water plane coefficient

D_P Propeller diameter

J Propeller advance ratio

K_Q Propeller torque coefficient

K_T Propeller thrust coefficient

n_P Propeller rotational speed

t Thrust deduction factor

w Wake fraction

β Drift angle

δ_R Rudder angle

ϵ Ratio of wake fractions among rudder and propeller

ϵ_K Lift to drag angle

γ Flow rectification factor

ϕ_K Kite azimuth

ρ_a Air density

ρ_w Water densiy

θ_K Kite elevation

Subscripts

AW Apparant wind

C Current

HF High frequency motions

K Kite

LF Low frequency motions

P Propeller

R Rudder

RW Relative wind

S Ship

T Tether

W Wind

Mathematical Symbols

$\circ$ Hadamard product

$\overline{}$ Time average

$\times$ Cross product

1 Introduction

This work takes place within the research program of the beyond the sea® project to develop kites as auxiliary propulsion of ship for fuel saving. The first attempt of the project is to refit merchant ship, from fishing vessel to container ship, to set up a tethered kite. Consequently, the kite design depends on the ship characteristics from different perspectives such as maneuverability, stability and seakeeping. Here the purpose of this study is focused on the development of a strategy and dedicated tools to choose a good tether attachment point on the deck according to the course keeping.

Previously, ships towed by kite have been essentially studied for the purpose of fuel saving predictions. Naaijen and Koster in [11] and Leloup et al. in [10] have predicted fuel saving assuming an average kite towing force over a closed kite loop trajectory and solving the ship static equilibrium. In these two papers, the hydrodynamic forces have been modeled with hull derivatives of maneuvering model of the corresponding ship. The sway and yaw equilibrium have been checked for their cases of study. Naaijen

and Koster [11] studied a 50000 DWT tanker with a kite of 500 m^2 and Leloup et al. studied [10] the British Bombardier a tanker ship of 225 m long equipped with a kite of 320 m^2. Naaijen and Koster [11] explained that the tether should be attached at the bow of the ship. Nevertheless, the hull form of a fishing vessel is different from a tanker and the conclusions of these former studies may be affected.

Consequently, a general approach is proposed here. The dynamic of a ship towed by kite is solved numerically. Here, the study is limited to calm water. The maneuvering motions are modeled with the parametric model proposed by Yoshimura and Masumoto [18] validated with a wide range of ship from fishing vessels to container ships. Regarding the kite modeling, different level of approach are possible. The simpler one is the so-called zero-mass model introduced by Wellicome and Wilkinson [17]. Leloup et al.[10] provided its analytical formulation. In this model the mass of the kite is neglected with a straight and mass-less tether. Despite these strong assumptions, Dadd et al. in [5] have shown favorable comparison with experimental data and the zero-mass model. Here, this model is used due to its inexpensive computational cost.

First of all, the model of a ship towed by kite is introduced, and based on this model a general simplified method is presented. Then, a validation case of the maneuvering model is presented with full scale experiments performed on the Steven Paul a 13 m long fishing vessel equipped of a 50 m^2 kite by [2]. Finally, the influence of the tether attachment location on a fishing vessel course keeping ability is analysed.

2 Model of ship towed by kite

2.1 Ship modeling

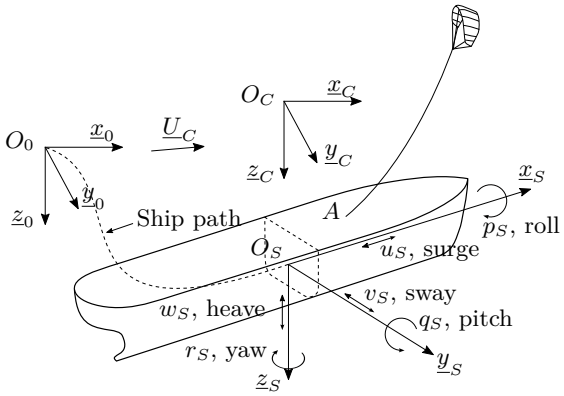

Figure 1 – Coordinates systems and ship motions

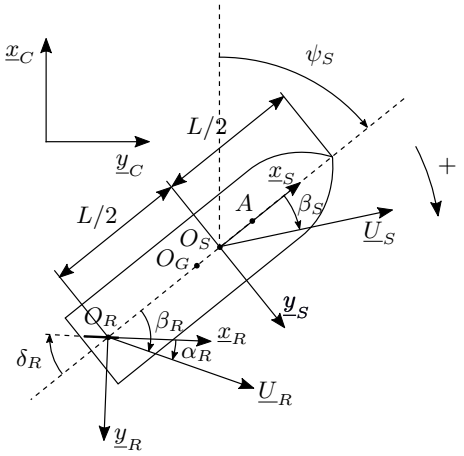

Figure 2 – Ship parametrization in the low frequency coordinates system $\mathcal{R}_{LF}$

The coordinates systems used to develop the model are represented in Figs. 1 and 2. $\mathcal{R}_0\left(O_0,\ \underline{x}_0,\ \underline{y}_0,\ \underline{z}_0\right)$ is the earth fixed coordinate system, using the North East Down (NED) convention. $\mathcal{R}_C\left(O_C,\ \underline{x}_C,\ \underline{y}_C,\ \underline{z}_C\right)$ is the current coordinate system. This frame has a rectilinear motion compared to $\mathcal{R}_0$ with a constant velocity vector $\underline{U}_C$. $\mathcal{R}_S\left(O_S,\ \underline{x}_S,\ \underline{y}_S,\ \underline{z}_S\right)$ is the ship coordinate axis system, rigidly fixed to the ship. $\underline{z}_S$ points downward, $\underline{x}_S$ points forward, and the $\underline{y}_S$ points to starboard. Its origin O_S is at mid-ship, in the intersection between the center plane of the boat and the free surface.

Eq. (1) defines the ship equation of motion with respect to the inertial frame $\mathcal{R}_C$ expressed in ship coordinates system $\mathcal{R}_S$ as formulated by Perez in [13].

$$\left[\underline{\underline{M}}_S + \underline{\underline{A}}_S(0)\right]\dot{\underline{V}}_S + \underline{\underline{C}}_S\underline{V}_S = \underline{F} \tag{1}$$

$\underline{\underline{M}}_S$ and $\underline{\underline{A}}_S(0)$ are the generalized mass matrix (6x6) and the added mass matrix (6x6) for zero-wave frequency. The added mass matrix $\underline{\underline{A}}_S(0)$ can be obtain by using the potential flow theory. $\underline{V}_S$ is the generalized ship velocity vector relative to $\mathcal{R}_C$ expressed in $\mathcal{R}_S$ at mid-ship. $\underline{V}_S$ is the assembly of the linear ship velocity $\underline{U}_S$ with the ship angular velocity $\underline{\Omega}_S$. $\dot{\underline{V}}_S$ is the generalized velocity time derivative. $\underline{\underline{C}}_S$ is the centripetal matrix (6x6). $\underline{F}$ is the generalized force vector representing the forces acting on the ship. $\underline{F} = \left[\ X, \ ,Y, \ Z, \ K, \ M, \ N \ \right]^T$, where the three first components of $\underline{F}$ represent the forces and the three last components represent the moments. The generalized force vector $\underline{F}$ can be decomposed into the sum of the hull, rudder, propeller and kite contributions such as in Eq. (2), where the subscripts $_H$, $_R$, $_P$, $_T$ and $_W$ denote respectively the hull, the rudder, the propeller, the appendages, the tether and windage.

$$\underline{F} = \underline{F}_H + \underline{F}_R + \underline{F}_P + \underline{F}_{APP} + \underline{F}_T + \underline{F}_W \tag{2}$$

The specification of this tool is to cover a wide range of ship, from small fishing vessels to large container ships. Many maneuvering models are available in the literature but only few of them are parametric. Yoshimura and Masumoto [18] proposed a parametric nonlinear maneuvering model. They developed parametric formulations of Taylor's expansions expressing the forces acting on the hull. This model is used here for its large range of validity, from fishing vessel of 26 m long to a container ship of 230 m long.

The expression of the propeller thrust is given by Eq. (3).

$$X_P = (1-t)\,\rho_w K_T D_P^4 n_p^2 \tag{3}$$

The thrust factor, denoted byK_T, is considered for an open water propeller. The thrust deduction factor is denoted by t. The thrust factor is function of the propeller advance ratio, denoted by J and expressed with the wake fraction w in Eq. (4).

$$J = (1-w)\,\frac{u_S}{n_P D_P} \tag{4}$$

The thrust deduction factor and the wake fraction can be determined with semi-empirical formulas such as those formulated by Weingart in Eq. (5) described in [8].

$$t = w\left(1.57 - 2.30\frac{C_B}{C_{WP}} + 1.50 C_B\right) \tag{5}$$

Where C_{WP} denotes the water plane coefficient and C_B denotes the hull block coefficient. The hull block coefficient is calculated with the mid-ship draft without considering the false keel in accordance with Yoshimura and Masumoto [18].

The rudder forces can be obtained according to the formulation proposed by Söding in [15]. This model has the advantage to be still valid for high angles of attack. The determination of the rudder inflow velocity is one of the most difficult task for naval engineers. Indeed, the inflow depends on the hull, the propeller and the rudder configuration and on the interactions between them. However, the determination of the exact inflow velocity into the whole fluid domain is not the objective here. Nevertheless, modeling these interactions cannot be avoided. Thus, it can be found in the literature several empirical formulas to describe the phenomena. Here, the formulation provided in Yoshimura and Masumoto [18], Eq. (6) is retained in order to have a parametric formulation of the interaction coefficients.

$$\begin{cases} u_{C,R} &= -u_S \epsilon\,(1-w)\sqrt{\eta\left[1 + \frac{k_x}{\epsilon}\left(\sqrt{1+C_{TH}} - 1\right)\right]^2 + (1-\eta)} \\ v_{C,R} &= -\gamma\,(v_S - 0.9 L r_S) \end{cases} \tag{6}$$

The dependency of the rudder inflow velocity with propeller thrust is modeled with the interactions coefficients ϵ and k_x defined with semi-empirical formulas by Yoshimura and Masumoto [18]. η denotes the geometric ratio between the propeller diameter and the rudder span, $\eta = {}^{D_P}/_{b_R}$. Downstream from

the propeller the axial flow velocity increases, which can be noticed with Eq. 6. The axial rudder inflow velocity increases with the propeller thrust loading coefficient $C_{TH} = 8K_T/\pi J^2$.

The transverse rudder inflow velocity v_R depends on the ship turning rate and ship transverse velocity. The hull tends to decrease the absolute value of the transverse rudder inflow velocity. This effect is represented by Yoshimura and Masumoto with the flow rectification factor, γ in Eq. 6. For single screw ship, positive yaw rate maneuvers and negative yaw rate maneuvers are asymmetric. This effect can be taken into account with two flow rectification factor, γ^+ and γ^- respectively for positive and negative turning rate.

Blendermann in [4] provides a semi-empirical expression of the wind load on the deadworks of various types of vessel. Longitudinal, lateral wind load forces and yaw wind load moments are expressed by means of coefficient obtained with wind tunnel experiments.

2.2 Kite modeling

A kite is ordinary composed of soft and light material such as textile. The kite shape is basically dependent of its wind loading. An ideal kite model should take into account the complete fluid structure interaction with finite deformation. Nevertheless, a kite is very lightweight structure compared to its aerodynamic load. Consequently, numerous studies on the dynamic kite flight motions have been carried out with the so-called zero-mass model, for instance Wellicome and Wilkinson [17], Naaijen et al. [12], Dadd et al. [6] and Leloup et al. [10]. Moreover, Leloup et al. [10] provide an analytical formulation of the zero-mass model. This analytical formulation has the benefit to be fast to compute. The mass of the tether and the kite are neglected and the tether is assumed to be straight. Consequently, for any configurations the tether tension is opposed the aerodynamic kite force, Eq. (7).

$$\underline{T}_K = \underline{F}_{A/K} \tag{7}$$

Fig. 3 illustrates the notations used for the zero-mass model. $\mathcal{R}_{RW}$ is the relative wind coordinates system moving at the tether attachment point velocity. The relative wind velocity defined in Eq. (8) is the difference between the true wind velocity at the kite location and the velocity of the tether attachment point compared to $\mathcal{R}_0$. The direction of the relative wind velocity is $\underline{x}_{RW}$. $\underline{y}_{RW}$ is defined as: $\underline{y}_{RW} = \frac{\underline{z}_0 \times \underline{x}_{RW}}{\|\underline{z}_0 \times \underline{x}_{RW}\|}$. In order to define a direct orthonormal coordinates system $\underline{z}_{RW}$ is defined as follows: $\underline{z}_{RW} = \underline{x}_{RW} \times \underline{y}_{RW}$. The relative wind velocity to the tether attachment point $\underline{U}_{RW}$ and the apparent wind velocity to the kite $\underline{U}_{AW}$ relative to the kite are defined respectively in Eqns. (8) and (9).

$$\underline{U}_{RW} = \underline{U}_{TW} - \underline{U}_A - \underline{U}_C \tag{8}$$

$$\underline{U}_{AW} = \underline{U}_{RW} - \underline{U}_K \tag{9}$$

In order to represent the wind friction with the sea, the true wind velocity is function of the altitude according to the wind gradient law recommended by the ITTC [1]. The measurement altitude of the wind relative to the sea level is denoted by z_{ref}. The wind velocity at z_{ref} is denoted by $\underline{U}_{ref}$. The wind gradient parameter n is equal to 1/7 as recommended by [1].

$$\underline{U}_{TW} = \left(\underline{U}_{ref} - \underline{U}_C\right) \left(\frac{z_K^{(0)}}{z_{ref}^{(0)}} \right)^n + \underline{U}_C \tag{10}$$

For a given lift-to-drag ratio angle denoted by ϵ_K, a given kite velocity direction $\underline{x}_{VK}$, the kite velocity relative to the tether attachment point, is written Eq. (11).

$$\underline{U}_K = U_{RW} \left[\underline{x}_{VK} \cdot \underline{x}_{RW} + \sqrt{\left(\underline{x}_{VK} \cdot \underline{x}_{RW}\right)^2 + \left(\frac{\underline{z}_{K0} \cdot \underline{x}_{RW}}{\sin \epsilon_K} \right)^2 - 1} \right] \underline{x}_{VK} \tag{11}$$

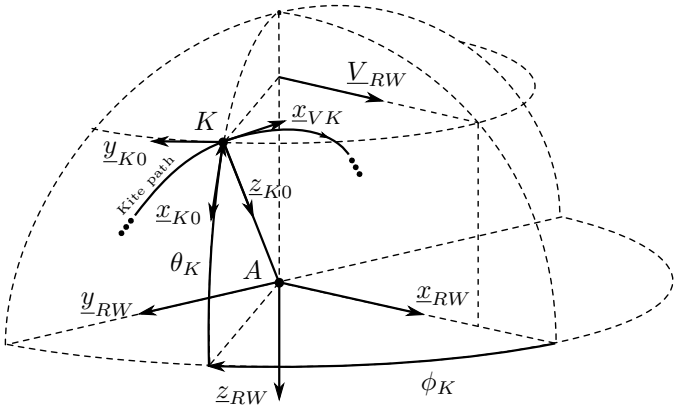

Figure 3 – Coordinate systems used for the development of the zero-mass model

Finally, the tether tension is given by the following formula:

$$\underline{T}_K = -\frac{C_{L_K}\rho_A A_K U_{AW}^2}{2\cos\epsilon_K}\underline{z}_{k0} \tag{12}$$

The generalized tether force vector acting on the ship at O_S is expressed as follows:

$$\underline{F}_K = \left[\begin{array}{cc} \underline{T}_K^{(S)} & \underline{O_S A}^{(S)} \times \underline{T}_K^{(S)} \end{array} \right]^T \tag{13}$$

2.3 Ship and kite control

During a simulation, rather than to constrain a degree of freedom, an automatic pilot is implemented in order to compute the required rudder angle to perform a maneuver or to follow a constant heading. The automatic pilot implemented is a PID-controller (Proportional Integrator Derivative) of the form proposed by Fossen in [7]. Based on this design of PID-controller, the propeller speed is control to reach a required ship velocity.

The kite velocity direction $\underline{x}_{VK}$ is controlled in order to perform eight trajectory. θ_{ref} and ϕ_{ref} are the elevation and azimuth of the trajectory on the sphere of center A and radius L_T. The center of the trajectory C_8 is positioned at $\left(\begin{array}{cc} \phi_8, & \theta_8 \end{array} \right)$. Eq. (14) defines elevation and azimuth of the eight parametric curve.

$$\begin{cases} \theta_{ref} & = \Delta\theta_8 \sin(2\xi) \\ \phi_{ref} & = \Delta\phi_8 \sin(\xi) \end{cases} \tag{14}$$

The eight trajectory can be rotated of an angle χ_8 around $\underline{C_8 A}$. For a given elevation θ_K and azimuth ϕ_K on a sphere of radius L_T, the corresponding cartesian coordinates in $\mathcal{R}_{RW}$ are defined as follows:

$$\left[\begin{array}{c} L_T \cos\theta_K \cos\phi_K \\ L_T \cos\theta_K \sin\phi_K \\ -L_T \sin\theta_K \end{array} \right] \tag{15}$$

2.4 Resolution of equations of motion

The equation of motion of the whole system is expressed in the form of a first order differential equation in Eq. (16).

$$\begin{bmatrix} \dot{\underline{V}}_S \\ \dot{\underline{X}}_S^{(C)} \\ \dot{\underline{X}}_K^{(C)} \end{bmatrix} = \begin{bmatrix} m_f \circ \left(\underline{\underline{M}}_S + \underline{\underline{A}}_S(0) \right)^{-1} \left(\underline{F} - \underline{\underline{C}}\,\underline{V}_S \right) \\ \begin{bmatrix} \underline{\underline{T}}_S^{(C)} & \underline{\underline{O}}_3 \\ \underline{\underline{O}}_3 & \underline{\underline{R}}_S^{(C)} \end{bmatrix} \underline{V}_S \\ \underline{U}_{RW} \left[\underline{x}_{VK} \cdot \underline{x}_{RW} + \sqrt{(\underline{x}_{VK} \cdot \underline{x}_{RW})^2 + \left(\frac{z_{K0} \cdot x_{RW}}{\sin \epsilon_K} \right)^2 - 1} \right] \underline{x}_{VK} + \underline{U}_A \end{bmatrix} \tag{16}$$

m_f is the considered degree of freedom vector. "$\circ$" is the Hadamard product. In this study, only surge sway and yaw motions are considered, consequently $m_f = [1,\ 1,\ 0,\ 0,\ 0,\ 1]^T$. For any vector, $\underline{x}$ expressed in $\mathcal{R}_S$, its image in $\mathcal{R}_F$ is obtained thanks to the direct cosine matrix $\underline{\underline{T}}_S$ as follows:

$$\underline{\underline{T}}_S = \begin{bmatrix} \cos\psi_S \cos\theta_S & \sin\psi_S \cos\theta_S & -\sin\theta_S \\ \sin\psi_S \cos\phi_S + \cos\psi_S \sin\theta_S \sin\phi_S & \cos\psi_S \cos\phi_S + \sin\psi_S \sin\theta_S \sin\phi_S & \cos\theta_S \sin\phi_S \\ \sin\psi_S \sin\phi_S + \cos\psi_S \sin\theta_S \cos\phi_S & -\cos\psi_S \sin\phi_S + \sin\psi_S \sin\theta_S \cos\phi_S & \cos\theta_S \cos\phi_S \end{bmatrix} \tag{17}$$

The ship angular velocity expressed in $\mathcal{R}_S$ is $\underline{\Omega}_S = [p_S,\ q_S,\ r_S]^T$. Eq. (18) is the relationship between the angular velocity and the time-derivatives Euler's angles.

$$\underline{\Omega}_S = \underline{\underline{R}}_C^{(S)} \dot{\underline{\Phi}}_S \tag{18}$$

Where, $\underline{\underline{R}}_C^{(S)}$ is:

$$\underline{\underline{R}}_C^{(S)} = \begin{bmatrix} 1 & 0 & -\sin\theta_S \\ 0 & \cos\phi_S & \cos\theta_S \sin\phi_S \\ 0 & -\sin\phi_S & \cos\theta_S \cos\phi_S \end{bmatrix} \tag{19}$$

The equations of motion are solved numerically with the 4^{th} order Runge-Kutta numerical scheme.

2.5 Simplified model

Since the kite can induce a yaw moment, an appropriate attachment position of the tether should be determined. Assuming that this appropriate position should keep the mean rudder angle at zero, the longitudinal attachment position of the tether x_A can be estimated according to this simplified approach. Considering the time average of the kite forces, the corresponding static equilibrium of the ship in surge sway and yaw can be simplified as follows:

$$\begin{cases} -R_{TBH}(u_s) + qLd_{em} \left(X'_{\beta_S \beta_S} \beta_S^2 + X'_{\beta_S \beta_S \beta_S \beta_S} \beta_S^4 \right) + \overline{X}_K + X_P & = 0 \\ qLd_{em} Y'_{\beta_S} \beta_S + \overline{Y}_K + 2\pi q A_R \beta_S & = 0 \\ qLd_{em} N'_{\beta_S} \beta_S + \frac{x_A}{L} \overline{Y}_K - \pi q A_R \beta_S & = 0 \end{cases} \tag{20}$$

Where q denotes the dynamic pressure, $q = \frac{1}{2}\rho_w U_S^2$. In Eq. (20) the longitudinal rudder force has been neglected. The interactions between the rudder and propeller have been neglected. The transverse rudder force is assumed to be equal to the lift of a plate without taking into account the 3D effects. Only the first order of the hydrodynamic sway force and hydrodynamic yaw moment have been taken into account. Consequently, considering the sway and yaw equilibrium equations, the tether attachment position leading to a zero rudder angle is given in Eq. (21).

$$x_A = L \frac{Ld_{em} N'_{\beta_S} - \pi A_R}{Ld_{em} Y'_{\beta_S} + 2\pi A_R} \tag{21}$$

According to the parametric hull derivatives formulas of Yoshimura and Masumoto [18], Eq. (21) becomes:

$$x_A = L\frac{2Ld_{em}^2\left(1-0.85\frac{t_S}{d_{em}}\right)-\pi A_R}{Ld_{em}\left(\pi d_{em}+1.4C_B B\right)\left(1+0.54\frac{t_S^2}{d_{em}^2}\right)+2\pi A_R} \tag{22}$$

Moreover the drift angle can be expressed as a function of the transverse kite force, Eq. (23).

$$\beta_S = \frac{-Y_K}{q\left(Ld_{em}Y'_{\beta_S}+2\pi A_R\right)} \tag{23}$$

According to the surge static equilibrium, the transverse kite force has a negative effect on fuel saving. Naaijen and Koster in [11] and Leloup et al. in [10] have neglected the drift motion induced by the kite for fuel saving calculation and for kite flight trajectory. Assuming, the drift angle is small, at the first order, $u_S \approx U_s$. Consequently, a simplified power saving ratio can be determined according to the simplified approach in Eq. (24).

$$\eta_K^* = \frac{q\left(X'_{\beta_S\beta_S}\frac{Y_K^2}{q^2\left(Ld_{em}Y'_{\beta_S}+2\pi A_R\right)^2}+X'_{\beta_S\beta_S\beta_S\beta_S}\frac{Y_K^4}{q^4\left(Ld_{em}Y'_{\beta_S}+2\pi A_R\right)^4}\right)+X_K}{R_{TBH}(u_s)} \tag{24}$$

3 Case of study and experimental setup

Figure 4 – Steven Paul fishing vessel

Figure 5 – beyond the sea® kite of 50 m^2

The case of study presented here is a 13 m long fishing vessel named Steven Paul (cf. Fig. 4) and equipped with a kite of 50 m^2(cf. Fig. 5). General characteristics of the system are resumed in Tab. 1.

The whole data acquisition system is based on a National Instruments CompactRIO platform. It consists of 3 main parts: a set of I/O modules depending on sensor technology, a Field-Programmable Gate Array (FPGA, NI CRIO-9114) and a Real-Time processor (NI CRIO-9024). All I/O modules are connected to the FPGA, and the very accurate clock of the FPGA ensures a good synchronization between the channels, and precise acquisition frequencies. The Real-Time processor logs all data coming from sensor through the FPGA on a non-volatile memory. To measure motions and velocities of the boat, an Inertial Measurement Unit (IMU) coupled with a Global Positioning System (GPS) was set up (Xsens MTi-G-700). This Unit includes a microprocessor able to realize data fusion, based on an extended Kalman filter providing roll and pitch information. Manufacturer ensures dynamic error for roll and pitch under 1° with a 1σ RMS error of 0.1°. The acquisition frequencies of the Xsens were 50Hz for inertial sensors (gyroscope and

Ship		Propulsion	
Length Overall	13.39 m	Motor	Caterpillar 3408 - 480hp
Length of waterline	12.89 m	Propeller	Kaplan 19-A 4 blades
Length between perpendiculars	12.28 m	Propeller diameter	1.30 m
Beam of the hull	5.61 m	Pitch ratio	1.015
Displacement	64 t	Blade area ratio	0.55
Mid-ship draft	1.75 m		
Trim	1.0 m		
Hull block	0.51		
Rudder		Kite	
Area	1.23 m^2	Area	50 m^2
Span	1.37 m	Lift to drag angle	9.46°
Chord	0.9 m	Lift coefficient	0.72
		Tether length	60 m

Table 1 – General characteristics of the fishing vessel Steven Paul (trial condition) and kite; The trim is defined in accordance to Yoshimura and Masumoto [18]

accelerometer), 20 Hz for roll and pitch, and 5Hz for all data regarding GPS technology (position and velocity). To avoid complex and unreliable calibration procedure of magnetometers, it has been decided to use an existing on board sensor to get yaw information, based on dual antenna GPS, instead of yaw information provided by the magnetometers of the Xsens IMU. The sensor was a Si-Tex Vector Pro, with 1σ RMS error under 0.3°.

A device measuring the torque on the propeller shaft, developed by the company UpDaq, had also been installed previously on board. A strain gauge had been stuck on the shaft and is linked to an amplifier, sending data wirelessly to a receiver in the wheelhouse. The latter was connected to the acquisition system through a serial link. The torque on the shaft was logged at 20Hz.

The measurement of rotational speed of the shaft propeller was carried out thank to a binary sensor, going from 0 V to 5 V each time the magnet stuck on the shaft passes nearby the sensor. The sensor was directly linked to the Digital Input module (NI 9411) of the compactRIO system. The rotational speed of the shaft was logged at 20Hz

4 Maneuvering model validation without kite

The resistance and the power characteristics are identified with the experimental data collected during a power test. For five different quasi-steady states of engine power, the ship velocity over ground, the propeller rotational speed and the torque on the shaft are measured. In order to obtain the ship velocity with respect to the free surface, the current velocity $\underline{U}_C$ is identified according to the IMO Resolution A.751 (1993) with a turning circle done just before the power test. For each steady state the torque coefficient can be identified with the following relationship:

$$K_Q^{exp} = \eta_{SSB} \frac{\overline{Q}_{SSB}^{exp}}{\rho_w \overline{n}_P^{exp^2} D_P^5} \tag{25}$$

Where, $\overline{Q}_{SSB}^{exp}$ denotes the torque measured on the propeller shaft after the shaft stuffing box and η_{SSB} denotes the shaft stuffing box efficiency. The shaft stuffing box efficiency is assumed to be equal to 0.97 as recommended by Bertram in [3]. Assuming that the Steven Paul propeller is equivalent to Kaplan 19-A of diameter 1.30 m, of pitch ratio of 1.015 and of blade area ratio of 0.55, the wake fraction is estimated according to Eq. (26) for each quasi-steady state of the power test:

$$K_Q^{exp} = K_Q \left(J = (1-w) \frac{\overline{u}_S^{exp}}{\overline{n}_P^{exp} D_P} \right) \tag{26}$$

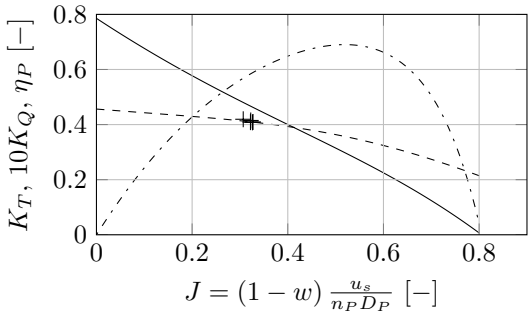

Figure 6 – Comparison between experimental data (denoted by + symbol) and model of the torque coefficient (dashed line) as a function of the propeller advance ratio J. The solid line shows the propeller thrust coefficient K_T and the dash-dotted line shows the propeller efficiency η_P by Kuiper [9]

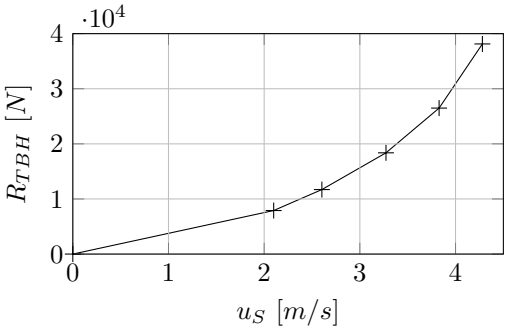

Figure 7 – Total resistance of the bare hull of the Steven Paul calculated with the presented method

The torque coefficient denoted by K_Q is determined according to the regression model proposed by Kuiper [6]. Consequently the estimated value of the wake fraction is 0.39. The left hand side and the right hand side of the system in Eq. (26) are plotted in Fig. 6. The predicted wake fraction according to the semi-empirical formula of Hecksher for trawlers, described in [3], is $w = 0.32$. The estimated value of the wake fraction is higher than predicted by Hecksher but this can be explained by the presence of a protection cage upstream of the propeller. This cage may drastically decrease the mean inflow velocity on the propeller disk area. According to Eq. (5) a thrust deduction factor of 0.34 is obtained. Finally, the total resistance of the bare hull in Eq. (27) is plotted in Fig. 7.

$$R_{TBH} = \frac{(1-t)\,K_T}{D_P K_Q^{exp}} \eta_{SSB} Q_{SSB}^{exp} + X + X_{APP} \tag{27}$$

In order to validate the Steven Paul maneuvering model, one turning circle of each side has been tested. The ship motions during the maneuvers are computed using the experimental rudder angle and the experimental propeller rotational speed as inputs. The two time series at the bottom of Fig. 9 represent respectively the experimental rudder angle and the propeller rotational speed. In addition, in Fig. 9, ship velocity (surge and sway) and yaw turning rate are plotted. The computed ship path and the measured ship path are compared in Fig. 8.

It can be noticed an important asymmetry between the port-side turning circle (denoted by triangle markers) and starboard turning circle (denoted by circle marker), therefore custom values of the flow rectification factor has been used for each turning sides, $\left(\ \gamma^+,\ \gamma^+\ \right) = \left(\ 0.92,\ 0.70\ \right)$. These values have been optimized in order to obtain the same turning radius than the trials. According to the semi-empirical formula of Yoshimura and Masumoto in [18], the mean flow rectification factor is 0.63.

The transient part until 10 s and the steady part after 10 s can be distinguished. A good agreement can be noticed for the surge and sway velocity and the yaw turning rate during the steady part of the motion. Regarding the transient part of the turning circle, the decelerating of the simulated surge velocity is lower than the experiments especially on port-side. Moreover, a delay is observable in term of yaw motion in Fig. 9, which is confirmed in term of ship path. Despite the observable differences, especially for the transient part, the maneuvering model is satisfactory according to the measurements uncertainties and the usual maneuvering validation results available in the literature Stern et al. [16].

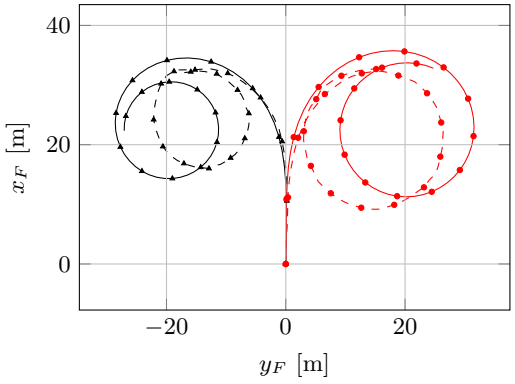

Figure 8 – Ship path during a turning circle to port board in the current coordinates system; Dashed and solid lines denote respectively the experimental data and simulated data; black triangle and red circle marks denote respectively the turning circles to portside and to starboard

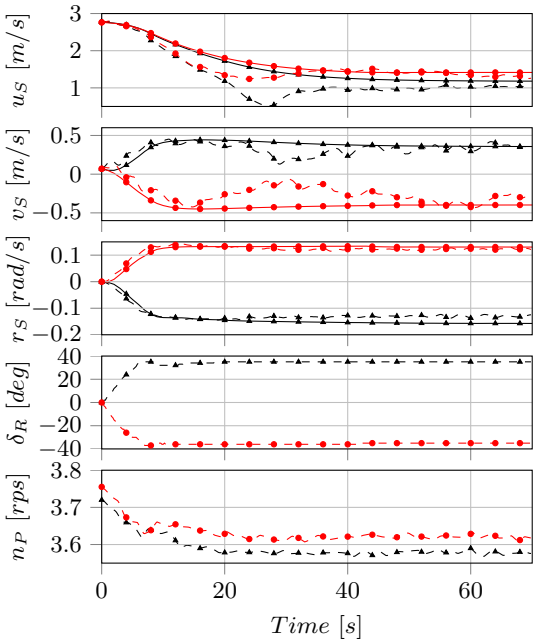

Figure 9 – From the top to the bottom respectively time series of: surge and sway velocity; yaw turning rate; rudder angle; propeller revolution per second. Dashed and solid lines denote respectively the experimental data and simulated data; black triangle and red circle marks denote respectively the turning circles to portside and to starboard

5 Course keeping results

The results are computed for the Steven Paul cruising speed of 3.5 m.s^{-1}. The true wind angle sets for the case of study is $\beta_{TW} = 135°$ and with true wind speed of 7.5 m.s^{-1}at an altitude of measurement of 10 m. This wind wind condition is favorable for the use of a kite in a dynamic flight. The eight trajectory azimuth amplitude and elevation amplitude are arbitrary set to respectively $\Delta\phi_8 = 40°$ and $\Delta\theta_8 = 8°$. According to Eq. (24), the center of trajectory and the trajectory orientation are optimized with a Bayesian process routine implemented in Python [14]. The optimal center of trajectory is $C = (23.3°, 20.4°)$ and the optimal trajectory orientation is $\chi_8 = 0°$. With this simplified approach the simplified power saving ratio (cf. Eq. 24) is $\eta_K^* = 34.2\%$ and the expected drift angle (cf. 23) is $\beta_S = 3.0°$. According to Eq. (22), the longitudinal tether attachment position leading to a zero mean rudder angle is $x_A = 1.76$ m with respect to O_S at mid-ship.

According to the full presented model, the ship motions have been computed with three different longitudinal attachment positions. The first one is the actual position of the experimental system settled up on the Steven Paul $x_A = 3.2$ m. The second one is computed with a tether attachment position on the deck leading to zero mean rudder angle, $x_A = 1.2$ m and the third one is at mid-ship, $x_A = 0.0$ m. Roll, pitch and heave motions are not considered. The propeller speed and the rudder angle are controlled by an autopilot. These results are computed with a time step of 0.05 s over 200 s of motion simulated. Only the last 20 s of simulation are presented in order to avoid the transient part. In Fig. 10, from top to bottom the drift angle, the rudder angle and the power saving ratio are plotted against time.

The power saving ratio is defined by Eq. 28, where W_{Q_P} is the power delivered by the propeller with kite and $W^*_{Q_P}$ is the power delivered by the propeller without kite.

$$\eta_K = \frac{W^*_{Q_P} - W_{Q_P}}{W^*_{Q_P}} \tag{28}$$

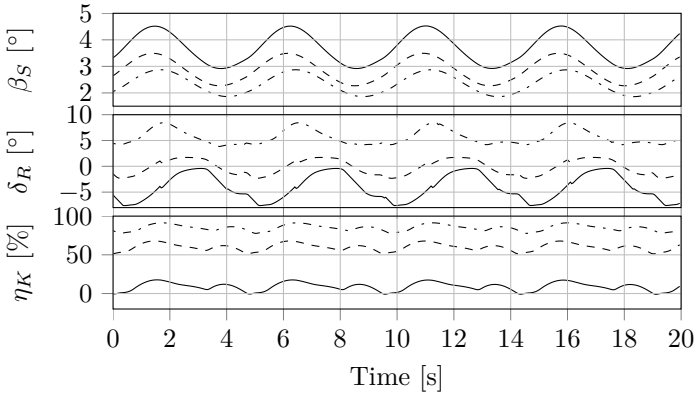

Figure 10 – From the top to the bottom: drift angle β_S, rudder angle δ_R, power saving ratio η_K; ···· configuration $x_A = 0.0$ m; - - - configuration $x_A = 1.2$ m; —— configuration $x_A = 3.2$ m

Tether attachment position x_A		0.0 m	1.20 m	3.2 m
Drift angle β_S	Average	2.35°	2.86°	3.68°
Rudder angle δ_R	Average	5.6°	-0.22°	-4.09°
	Amplitude	4.61°	4.05°	7.20°
Power saving ratio η_K	Average	84.71 %	59.85 %	8.85 %

Table 2 – Time average values of the the ship motions and rudder angle amplitude

The mean values of the simulated motions are reported in Tab 2.

6 Discussion

According to the simplified analysis the expected longitudinal position of the tether leading to zero mean rudder angle should be $x_A = 1.76$ m, with associated drift angle of 3°. With the dynamic simulations this attachment point is further back at $x_A = 1.2$ m corresponding roughly to the same drift angle of 2.86°. This result can be verified in Fig. 10, the rudder angle oscillates around $\delta_R = -0.22°$. Indeed, the propeller rudder hull interactions effects are not taken into account by the simplified analysis. Nevertheless the corresponding drift angle is correctly estimate with the simplified method compared to dynamic simulation. According to the maneuvering model derivatives of Yoshimura and Masumoto [18], the first order of the transverse force induced by the drift seems to be enough to correctly evaluate the drift angle. The simplified power saving ratio (cf. Eq. (24)) should not be used directly to evaluate the power saving since the propeller efficiency is not considered. However, this simplified power saving ratio may be convenient to optimize the kite trajectory.

The study on different tether attachment position shows that the power saving increase with a backward tether attachment point. With the actual tether position on the Steven Paul, $x_A = 3.2$ m forward to the mid-ship, the mean power saving is 8.85 %, whereas with further backward position the mean power saving increase drastically to 59.85 % with $x_A = 1.2$ m and to 84.71 % with $x_A = 0.0$ m. This could be explained with the drift angle and the rudder angle. The more the tether position is backward, the lower is the absolute mean value of the drift angle and higher is rudder angle. With the actual tether position $x_A = 3.2$ m the ship is lee helm, therefore the rudder angle is negative to counteract the yaw kite moment. Consequently, the transverse force of the rudder is positive leeward to the ship as the transverse kite force. Only the hydrodynamic hull transverse force due to the drift can counteract this two positive leeward transverse forces. On the contrary, with a weather helm ship the rudder and the hull counteract the kite transverse force. Therefore, the absolute value of the drift angle is higher for a weather helm ship than for a lee helm ship. Power saving is drastically higher on a weather helm ship than for lee helm ship. Another possibility to decrease the drift angle could be to add a centerboard.

In Tab. 2, it can be observed that the lower rudder angle amplitude is with a tether attachment point

at $x_A = 1.2$ m. An optimal tether attachment point can be found to limit the necessary rudder angle. With this approach, the rudder angle amplitude depends on the autopilot. Nevertheless, this highlights the importance to design dedicated rudder and dedicated automatic pilot for ship towed by kite.

Further investigations should be achieved in order to increase the power saving and to increase course-keeping stability. Two angles can be highlight to study this issue, one on the general design of the ship and an other on the control of the ship.

7 Conclusion

A model and a numerical scheme has been presented to take into account the low frequency motion induced by the kite. A validation of the maneuvering model has been done on Canadian fishing vessel equipped of kite. A simplified approach to evaluate the drift angle and the tether attachment point has been developed. This simplified approach enables to predict with good agreement the mean drift angle compared to the result given by the dynamic model. Moreover, according to this simplified approach an objective function has been developed to optimize the kite trajectory taking into account the ship resistance induced by the drift motion. The analysis of the influence of the longitudinal tether attachment point on the deck shows a high sensitivity on the power saving. More precisely, the mean rudder angle for course keeping and drift angle can drastically change the power saving. The importance of the tether attachment position on course keeping and performance has been shown and assessed for three cases. The computation of the motions shows that the more the tether attachment is backward, the more the propeller power required is low for the cases tested. For a given autopilot, the study shows that it exists an optimal tether attachment point to limit the rudder angle oscillation required for course keeping.

References

[1] ITTC Symbols and Terminology List Version 2014. Technical report, 2014.

[2] M. Behrel, N. Bigi, K. Roncin, D. Grelon, F. Montel, A. Nême, J. B. Leroux, C. Jochum, and Y. Parlier. Measured Performance of a 50-m2 Kite on a Trawler. In *High-Performance Marine Vehicles Conference*, 2016.

[3] V. Bertram. *Practical ship hydrodynamics*. Elsevier, 2012.

[4] W. Blendermann. Parameter identification of wind loads on ships. *Journal of Wind Engineering and Industrial Aerodynamics*, 51:339–351, 1994.

[5] G. M. Dadd, D. A. Hudson, and R. A. Shenoi. Comparison of two kite force models with experiment. *Journal of aircraft*, 47(1):212–224, jan 2010.

[6] G. M. Dadd, D. A. Hudson, and R. A. Shenoi. Determination of kite forces using three-dimensional flight trajectories for ship propulsion. *Renewable Energy*, 36(10):2667–2678, oct 2011.

[7] T. I. Fossen. *Marine control systems: guidance, navigation and control of ships, rigs and underwater vehicles*. Marine Cybernetics, 2002.

[8] J. M. J. Journée. Prediction of Speed and Behaviour of a Ship in a Seaway. *ISP*, 23(265):1–24, 1976.

[9] G. Kuiper. *The Wageningen propeller series*. Marin, 1992.

[10] R. Leloup, K. Roncin, M. Behrel, G. Bles, J.-B. Leroux, C. Jochum, and Y. Parlier. A continuous and analytical modeling for kites as auxiliary propulsion devoted to merchant ships, including fuel saving estimation. *Renewable Energy*, 86:483–496, 2016.

[11] P. Naaijen and V. Koster. Performance of auxiliary wind propulsion for merchant ships using a kite. In *2nd International Conference on Marine Research and Transportation*, pages 45–53, 2010.

[12] P. Naaijen, V. Koster, and R. P. Dallinga. On the power savings by an auxiliary kite propulsion system. *International shipbuilding progress*, 53:255–279, 2006.

[13] T. Perez. *Ship Motion Control; Course Keeping and Roll Stabilization Using Rudder and Fins*. Springer Science & Business Media, 2005 edition, 2005.

[14] J. Snoek, H. Larochelle, and R. P. Adams. Practical bayesian optimization of machine learning algorithms. *Advances in neural information processing systems*, pages 2951–2959, 2012.

[15] H. Soding. Limits of Potential Theory in Rudder Flow Predictions. *Ship Technology Research*, 45:141–155, 1998.

[16] F. Stern, K. Agdrup, S. Y. Kim, A. C. Hochbaum, K. P. Rhee, F. H. H. A. Quadvlieg, P. Perdon, T. Hino, R. Broglia, and J. Gorski. Experience from SIMMAN 2008 - the first workshop on verification and validation of ship maneuvering simulation methods. *Journal of Ship Research*, 55:135–147, 2011.

[17] J. F. Wellicome and S. Wilkinson. Ship propulsive kites: an initial study. 1984.

[18] Y. Yoshimura and Y. Masumoto. Hydrodynamic Database and Manoeuvring Prediction Method With Medium High-Speed Merchant Ships and Fishing Vessels. *Proceedings of International MARSIM Conference*, 2012.